Journal of Advanced Ceramics
2015, **4**(2): 83–93
DOI: 10.1007/s40145-015-0140-6

ISSN 2226-4108
CN 10-1154/TQ

Research Article

Theoretical prediction on mechanical and thermal properties of a promising thermal barrier material: $Y_4Al_2O_9$

Yanchun ZHOU*, Huimin XIANG, Xinpo LU, Zhihai FENG, Zhongping LI

Science and Technology of Advanced Functional Composite Laboratory, *Aerospace Research Institute of Materials and Processing Technology*, *No. 1 South Dahongmen Road*, *Beijing 100076*, *China*

Received: January 17, 2015; Accepted: January 24, 2015

Abstract: The mechanical and thermal properties of $Y_4Al_2O_9$ were predicted using a combination of first-principles and chemical bond theory (CBT) calculations. Density functional theory (DFT) computations were performed for the structural, mechanical, and thermal properties, and the results were confirmed by chemical bond theory. Based on the calculated equilibrium crystal structure, heterogeneous bonding nature has been revealed, i.e., Al–O bonds are stronger than Y–O bonds. Low second-order elastic constants c_{44}, c_{55}, and c_{66} demonstrate the low shear deformation resistance. Low G/B ratio suggests that $Y_4Al_2O_9$ is a damage tolerant ceramic. $Y_4Al_2O_9$ shows anisotropy in elastic behavior based on the discussion of direction dependence of Young's modulus. The hardness is predicted to be 10.2 GPa from calculated elastic moduli. The thermal expansion coefficient (TEC) calculated by chemical bond theory is 7.51×10^{-6} K^{-1}. In addition, the minimum thermal conductivity of $Y_4Al_2O_9$ is estimated to be 1.13 $W\cdot m^{-1}\cdot K^{-1}$, and the thermal conductivity decreases with temperature as $1305.6/T$.

Keywords: $Y_4Al_2O_9$; chemical bonding; elastic constants; thermal conductivity; thermal expansion coefficient (TEC)

1 Introduction

Yttria-stabilized zirconia (YSZ) is a widely used thermal barrier coating on turbine blades in gas-turbine engines to increase the operating temperature and the efficiency and power of the engines [1]. However, the instability of metastable tetragonal-prime structure due to the decomposition into a mixture of tetragonal and cubic zirconia limits the application of YSZ at higher operating temperatures [2]. Thus, searching for new thermal barrier coating (TBC) materials with low thermal conductivity, low density, low oxygen diffusivity, good high temperature stability, and ability to tailor mechanical damage is of virtual importance and has been the task of many investigations [3,4].

Recent works have demonstrated that yttrium aluminates are promising candidates for TBCs due to their superior high temperature stability, and mechanical and thermal properties [5,6]. At high temperatures, yttrium aluminum garnet (i.e., $Y_3Al_5O_{12}$, YAG) is stable with Al_2O_3 [5], which is the thermally grown oxide formed on Ni-based superalloys. Low thermal conductivity of YAG has been confirmed by Zhan *et al.* [7] very recently. Besides YAG, $Y_4Al_2O_9$ (YAM) is also a stable compound in the Y–Al–O

* Corresponding author.
E-mail: yczhou@imr.ac.cn

system [8]. The melting point of YAM is 2020 ℃, which is higher than that of YAG (1940 ℃). In addition, YAM has a low density of 4.44 g/cm^3, a relative low Young's modulus of 190 GPa, and a low minimum thermal conductivity of 1.10 W·m^{-1}·K^{-1} [7]. The unique combination of these properties makes YAM a promising TBC material for high temperature applications.

In our previous work, the minimum thermal conductivity of YAM was predicted and low thermal conductivity was experimentally confirmed [7]. The second-order elastic constants and the bulk modulus, shear modulus, and Young's modulus were also calculated [7]. Low thermal conductivity and high temperature stability were also confirmed by Zhou *et al.* [9] very recently. In addition, the point defects formation mechanism in YAM was investigated by Li *et al.* [10]. However, systematic investigation on the mechanical and thermal properties of YAM is still lacking. Clear understanding of mechanical and thermal properties and correlation of these properties to the structure of YAM can provide valuable insights for the development of TBCs and advance the applications of YAM as high temperature structural component and TBCs.

In this contribution, the structure, mechanical, and thermal properties of YAM were investigated from a combination of first-principles calculations and an empirical method based on chemical bond theory. The equilibrium crystal structure, second-order elastic coefficients, bulk modulus, shear modulus, Young's modulus, and Poisson's ratio were calculated by first-principles calculations. Then, the theoretical minimum thermal conductivity was estimated from modified Clarke's model [11,12], and the dependence of thermal conductivity of $Y_4Al_2O_9$ on temperature was predicted from Slack's model [13]. To valid the theoretical calculation, bulk modulus of YAM was also estimated using chemical bond theory. Then the average linear thermal expansion coefficient (TEC) was obtained using this empirical method.

2 Computation methods

2. 1 First-principles calculations

The first-principles calculations based on the density functional theory (DFT) were performed using the Cambridge Serial Total Energy Package (CASTEP) code [14], wherein the Vanderbilt-type ultrasoft pseudopotential [15] was employed. The electronic exchange-correlation energy was treated under the local density approximation (LDA) [16]. The plane-wave basis set cut-off energy was fixed at 450 eV. The special points sampling integration over Brillouin zone was realized by using the Monkhorst–Pack method with special *k*-points meshes of 4 × 2 × 2 [17].

To get the equilibrium crystal structure, the lattice parameters and internal atomic coordinates were independently modified. The free enthalpy, interatomic forces, and stresses of the unit cell were minimized under the Broyden–Fletcher–Goldfarb–Shanno (BFGS) minimization scheme [18]. The tolerances for geometrical optimization were: differences for total energy within 5×10^{-6} eV/atom, maximum ionic Hellmann–Feynman force within 0.01 eV/Å, maximum ionic displacement within 5×10^{-4} Å, and maximum stress within 0.02 GPa.

The theoretical elastic coefficients were determined from the first-principles strain–stress relationships' method implemented by Milman and Warren [19]. The criteria for convergence of optimization on atomic internal freedoms were selected as differences in the total energy within 1×10^{-6} eV/atom, Hellmann–Feynman force within 0.002 eV/Å, and maximum ionic displacement within 1×10^{-4} Å. The compliance tensor S was calculated as the inverse of the stiffness matrix, $S=C^{-1}$. The bulk modulus B and shear modulus G were calculated from the compliance tensor based on Voigt–Reuss–Hill approximation [20–22]. The Young's modulus E and Poisson's ratio ν were calculated using Hill's bulk modulus B_{H} and shear modulus G_{H} by the following equations [23]:

$$E=\frac{9B_{\mathrm{H}}G_{\mathrm{H}}}{3B_{\mathrm{H}}+G_{\mathrm{H}}} \tag{1}$$

$$\nu=\frac{3B_{\mathrm{H}}-2G_{\mathrm{H}}}{2(3B_{\mathrm{H}}+G_{\mathrm{H}})} \tag{2}$$

According to Slack's model [13] and modified Clarke's model [11,12], the behavior of thermal conductivity of a material at elevated temperatures is accessible. Slack's model describes the intrinsic thermal conductivity of a material over a wide range of temperature, which is expressed as [13]:

$$\kappa_{\mathrm{L}}=A\frac{\bar{M}\Theta_{\mathrm{D}}\delta^3}{\gamma^2n^{2/3}T} \tag{3}$$

where n is the number of atoms in the primitive unit cell; δ^3 is the volume per atom; Θ_{D} is the Debye

temperature; $\bar{M}$ is the average mass of the atoms in the crystal; and A is a physical constants ($A \approx 3.1\times10^{-6}$ if κ_L is in $W\cdot m^{-1}\cdot K^{-1}$ and δ in Å). High temperature limit of the acoustic phonon mode Grüneisen parameter γ, is a direct measure of the anharmonicity of phonon, and can be derived from Poisson's ratio [24]:

$$\gamma = \frac{9\left(\upsilon_l^2 - \frac{4}{3}\upsilon_s^2\right)}{2\left(\upsilon_l^2 - 2\upsilon_s^2\right)} = \frac{3}{2}\left(\frac{1+\nu}{2-3\nu}\right) \quad (4)$$

According to the modified Clarke's model [11,12], the theoretical lower limit of intrinsic thermal conductivity (κ_{min}) can be calculated by

$$\kappa_{min} \to k_B \upsilon_m \left(\frac{M}{ndN_A}\right)^{-2/3} \quad (5)$$

where k_B is the Boltzmann's constant; υ_m the average sound velocity; N_A the Avogadro's number; d the density; M the molecular weight; and n the number of atoms in the molecule. This modified model has been successfully applied to estimate the κ_{min} of several complex oxides, such as $La_2T_2O_7$ [12], MP_2O_7 [25], MPO_4 [26], β-$Yb_2Si_2O_7$ [27], $Yb_3Al_5O_{12}$ [28], and Yb_2SiO_5 [29].

The average sound velocity υ_m of a polycrystalline material is defined as the following [30]:

$$\upsilon_m = \left[\frac{1}{3}\left(\frac{2}{\upsilon_s^3} + \frac{1}{\upsilon_l^3}\right)\right]^{-1/3} \quad (6)$$

where υ_l and υ_s are longitudinal and transverse sound velocities, respectively, which can be determined from the shear modulus G and the bulk modulus B by

$$\upsilon_l = \sqrt{\frac{B + 4G/3}{d}} \quad \text{and} \quad \upsilon_s = \sqrt{G/d} \quad (7)$$

The Debye temperature, Θ_D, was calculated according to the following equation [30]:

$$\Theta_D = \frac{h}{k_B}\left[\frac{3n}{4\pi}\left(\frac{N_A d}{M}\right)\right]^{1/3} \upsilon_m \quad (8)$$

where h is the Plank's constant; k_B is the Boltzmann's constant; n is the number of atoms in the molecular formula; N_A is the Avogadro's number; d is the theoretical density; and M is the molecular weight.

2. 2 Chemical bond theory

Developed by Phillips and Van Vechten [31], Van Vechten [32], Levine [33], and Xue and Zhang [34], complex chemical bond theory (CBT) provides a simple but efficient approach to study the characteristic of chemical bonds in complex materials, and predicts related physical properties of a crystal from the viewpoint of bonding. The implementation of this theory relies on the decomposition of complex crystal into a linear combination of subformula of various binary crystals [34]. For a given chemical formula of a complex crystal, CBT provides an efficient way to decompose it into the following simple subformulas [34]:

$$A_{a1}^1 A_{a2}^2 \cdots A_{ai}^i B_{b1}^1 B_{b2}^2 \cdots B_{bj}^j = \sum_{i,j} A_{mi}^i B_{nj}^j = \sum_{\mu} (A_m B_n)^{\mu} \quad (9)$$

$$mi = \frac{N(B^j - A^i)\times ai}{N_C(A^i)} \quad \text{and} \quad nj = \frac{N(A^i - B^j)\times bj}{N_C(B^j)} \quad (10)$$

where $N_C(A^i)$ and $N_C(B^j)$ represent the coordination numbers of A^i and B^j ions in the crystal, respectively. $N(B^j - A^i)$ is the nearest coordination fraction contributed by A^i ion and *vice versa*. $(A_m B_n)^{\mu}$ is one of the subformulas.

For every fictitious binary crystal $(A_m B_n)^{\mu}$ decomposed according to CBT, the total lattice energy U^{μ} can be separated into the ionic part (U_i^{μ}) and the covalent part (U_c^{μ}), which can, respectively, be expressed as [35]:

$$U_i^{\mu} = \frac{1270(m+n)Z^+Z^-}{l^{\mu}}\left(1 - \frac{0.4}{l^{\mu}}\right) f_i^{\mu} \quad (\text{kJ}\cdot\text{mol}^{-1}) \quad (11)$$

$$U_c^{\mu} = 2100m\frac{(Z^+)^{1.64}}{(l^{\mu})^{0.75}} f_c^{\mu} \quad (\text{kJ}\cdot\text{mol}^{-1}) \quad (12)$$

where Z^+ and Z^- are the valences of cation and anion in the binary crystal, respectively; l^{μ} is the length of μ type bond. f_i^{μ} and f_c^{μ} are the ionicity and covalency of *A*–*B* bond, respectively, and are defined as [33]:

$$f_i^{\mu} = \frac{(C^{\mu})^2}{(E_g^{\mu})^2} \quad \text{and} \quad f_c^{\mu} = \frac{(E_h^{\mu})^2}{(E_g^{\mu})^2} \quad (13)$$

$$f_i^{\mu} + f_c^{\mu} = 1 \quad (14)$$

where E_g^{μ} is the average energy band gap and is composed of homopolar (E_h^{μ}) and heteropolar (C^{μ}) parts. These two parts of energy can be estimated by [33]:

$$E_h^{\mu} = \frac{39.74}{(l^{\mu})^{2.48}} \quad (\text{eV}) \quad (15)$$

$$C^{\mu} = 14.4b^{\mu}\exp(-k_s^{\mu}r^{\mu})\left[\frac{(Z_A^{\mu})^*}{r^{\mu}} - (n/m)\frac{(Z_B^{\mu})^*}{r^{\mu}}\right] \quad (\text{eV}) \quad (\text{if } n > m) \quad (16a)$$

$$C^{\mu}=14.4b^{\mu}\exp\left(-k_{s}^{\mu}r^{\mu}\right)\left[(m/n)\frac{(Z_{A}^{\mu})^{*}}{r^{\mu}}-\frac{(Z_{B}^{\mu})^{*}}{r^{\mu}}\right]\ \text{(eV)}$$

(if $m>n$) (16b)

where b^{μ} is a structural correction factor; $r^{\mu}=l^{\mu}/2$ is the average ion radius expressed in angstroms; $\exp(-k_{s}^{\mu}r^{\mu})$ is the Thomas–Fermi screening factor; $(Z_{A}^{\mu})^{*}$ and $(Z_{B}^{\mu})^{*}$ are the effective valence electron numbers of A and B ions, respectively.

The lattice energy density u^{μ} of a binary crystal, which is an essential parameter in estimating the bulk modulus and linear thermal expansion coefficient of a binary crystal, is defined as [36]:

$$u^{\mu}=\frac{U^{\mu}}{N_{A}n^{\mu}v_{b}^{\mu}} \tag{17}$$

where N_A is the Avogadro's constant; n^{μ} is the number of the chemical bond in one formula unit; and v_b^{μ} is the volume of μ type chemical bond. Then the bulk modulus B^{μ} of a certain type of binary crystals can be calculated on the basis of lattice energy density [36]:

$$B^{\mu}=\delta^{\mu}+\frac{u^{\mu}}{\beta^{\mu}} \tag{18}$$

where δ^{μ} is a constant; β^{μ} is a proportion factor depending on the average valence and average coordination number of subformula A_mB_n. The bulk modulus of the complex crystals is expressed as [37]:

$$B_{m}=\frac{1}{k_{m}} \tag{19}$$

$$k_{m}=\frac{\Delta V}{V_{m}\Delta P}=\frac{1}{V_{m}}\sum_{\mu}\frac{\Delta V_{\mu}}{\Delta P_{\mu}}=\frac{1}{V_{m}}\sum_{\mu}V^{\mu}k^{\mu}=\frac{1}{V_{m}}\sum_{\mu}\frac{V^{\mu}}{B^{\mu}} \tag{20}$$

where B^{μ} is the bulk modulus of μ type chemical bond; V^{μ} is the volume of μ type bond in one molecule.

The linear thermal expansion coefficient (TEC) of a complex crystal is closely related to the lattice energy and can be estimated by the following equations [38]:

$$\alpha=\sum_{\mu}F^{\mu}\alpha^{\mu} \tag{21}$$

$$\alpha^{\mu}=-3.1685+0.8376\chi^{\mu} \tag{22}$$

$$\chi^{\mu}=\frac{k_{\mathrm{B}}Z_{A}^{\mu}N_{\mathrm{CA}}^{\mu}}{U^{\mu}\Delta^{\mu}}\beta^{\mu}\ \text{ and }\ \beta^{\mu}=\frac{m(m+n)}{2n} \tag{23}$$

where parameter Δ^{μ} is a correction parameter from the analysis of experimental results, which depends on the position of cation in the periodic table. F^{μ} is the fraction of μ type bond in the complex crystal.

3 Results and discussion

3.1 Structural and chemical bonding properties

$Y_4Al_2O_9$ crystallizes in a monoclinic structure with a space group of $P2_1/c$. Figure 1(a) shows the crystal structure of $Y_4Al_2O_9$. It contains 60 atoms in the unit cell, which contains two Al sites, four Y sites, and nine O sites. The Al atoms are coordinated by four O atoms; Y(1), Y(3), and Y(4) atoms are coordinated with seven O atoms, and Y(2) is coordinated by six O atoms.

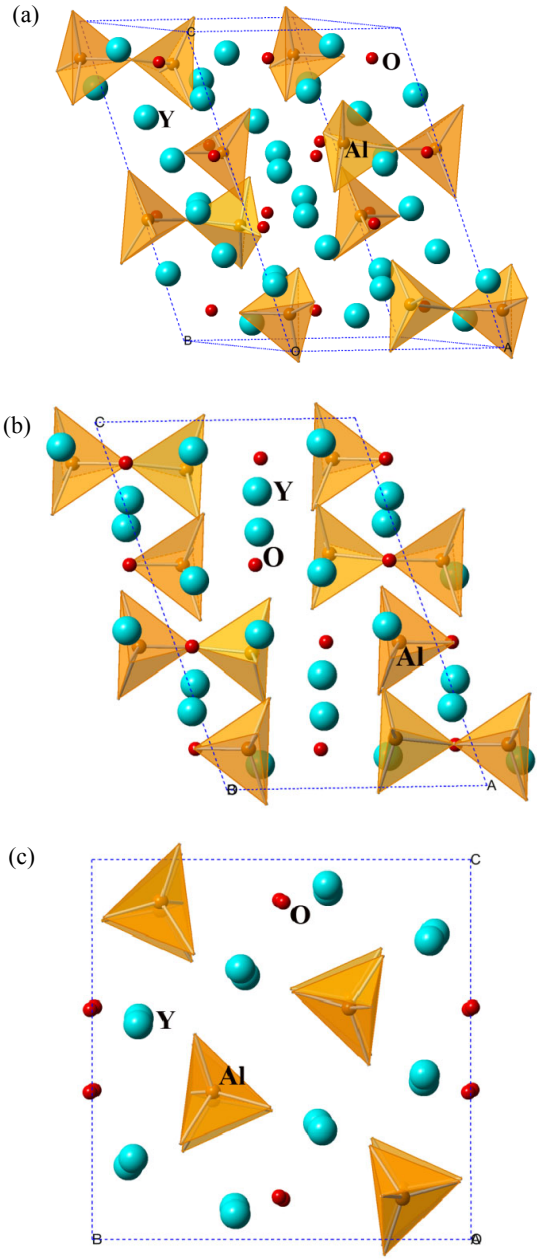

Fig. 1 (a) Crystal structure of $Y_4Al_2O_9$, (b) projection of atoms on (010) plane, and (c) projection of atoms on (100) plane.

The calculated lattice parameters of $Y_4Al_2O_9$ using DFT are listed in Table 1, together with the previously reported experimental data [39] for comparison. As shown in Table 1, the calculated lattice parameters are very close to the theoretical ones calculated by Zhan *et al.* [7], but are smaller than the experimental data [39]. The smaller geometry optimized lattice constants can be understood from the following two aspects. First, the experimental data were obtained using high temperature neutron diffraction at 1791 K and the lattice constants are much larger than both the room temperature and ground state data due to the thermal expansion. Second, relatively low optimized lattice constants are common for most of LDA approximation. The optimized atomic positions of Al, Y, and O atoms are quite consistent to the experimental reported ones. Good coincidence between the theoretical and the experimental results ensures the reliability of our calculations.

The Mulliken analysis on Y–O and Al–O bonds of $Y_4Al_2O_9$ was also conducted by DFT calculations, and the data are listed in Table 2. The Mulliken populations of Al–O bonds are higher than that of Y–O bonds, indicating higher level of covalency of Al–O bonds.

Table 1 Theoretical and experimental lattice parameters of $Y_4Al_2O_9$

Lattice constants		
	Geometry optimized	High temperature neutron diffraction data [39]
a (Å)	7.2610	7.4804
b (Å)	10.3134	10.5462
c (Å)	10.9431	11.2058
β (°)	108.628	108.927
Atomic positions		
	Geometry optimized	High temperature neutron diffraction data [39]
Al(1)	(0.9543, 0.1701, 0.1239)	(0.950, 0.178, 0.126)
Al(2)	(0.4131, 0.1817, 0.1166)	(0.397, 0.186, 0.106)
Y(1)	(0.2677, 0.1125, 0.7866)	(0.275, 0.1034, 0.7850)
Y(2)	(0.7778, 0.0917, 0.8064)	(0.781, 0.0966, 0.8095)
Y(3)	(0.0905, 0.1332, 0.4410)	(0.084, 0.1260, 0.4256)
Y(4)	(0.5845, 0.1159, 0.4096)	(0.5914, 0.1183, 0.4224)
O(1)	(0.5326, 0.2261, 0.7482)	(0.524, 0.2210, 0.7507)
O(2)	(0.9758, 0.2398, 0.7652)	(0.986, 0.2393, 0.7607)
O(3)	(0.9303, 0.0119, 0.1403)	(0.940, 0.022, 0.7507)
O(4)	(0.8232, 0.2372, 0.9768)	(0.816, 0.237, 0.9800)
O(5)	(0.1820, 0.2221, 0.1182)	(0.178, 0.2145, 0.118)
O(6)	(0.3877, 0.2391, 0.9640)	(0.380, 0.2427, 0.9634)
O(7)	(0.4773, 0.0271, 0.1744)	(0.474, 0.0311, 0.1719)
O(8)	(0.8348, –0.0001, 0.3913)	(0.828, –0.0020, 0.391)
O(9)	(0.3103, –0.0036, 0.3937)	(0.317, –0.0092, 0.391)

Table 2 Mulliken population and bond lengths of $Y_4Al_2O_9$

Bond	Population	Length (Å)
Al(1)–O(3)	0.55	1.7067
Al(1)–O(4)	0.52	1.7093
Al(2)–O(1)	0.49	1.7115
Al(2)–O(7)	0.52	1.7145
Al(2)–O(6)	0.52	1.7185
Al(2)–O(5)	0.41	1.7266
Al(1)–O(5)	0.40	1.7326
Al(1)–O(2)	0.47	1.7344
Y(2)–O(1)	0.30	2.1759
Y(1)–O(8)	0.28	2.1814
Y(3)–O(8)	0.26	2.2130
Y(3)–O(8)	0.27	2.2242
Y(4)–O(8)	0.26	2.2265
Y(2)–O(2)	0.27	2.2284
Y(4)–O(4)	0.28	2.2328
Y(1)–O(3)	0.36	2.2445
Y(3)–O(2)	0.28	2.2537
Y(1)–O(6)	0.26	2.2568
Y(1)–O(7)	0.28	2.2656
Y(2)–O(9)	0.33	2.2670
Y(2)–O(3)	0.33	2.2682
Y(2)–O(7)	0.26	2.2743
Y(4)–O(6)	0.24	2.2764
Y(4)–O(9)	0.30	2.2904
Y(3)–O(9)	0.32	2.2958
Y(2)–O(4)	0.23	2.3288
Y(4)–O(1)	0.21	2.3378
Y(4)–O(9)	0.26	2.3468
Y(3)–O(5)	0.19	2.3640
Y(1)–O(1)	0.21	2.3884
Y(1)–O(2)	0.18	2.4283
Y(1)–O(5)	0.18	2.4354
Y(3)–O(6)	0.15	2.4703
Y(7)–O(4)	0.17	2.4756

For $Y_4Al_2O_9$, the chemical bonds are diverse in length and covalency; the bond strength and bond energy are anticipated to be miscellaneous. To quantify this diversity, the chemical parameters, such as covalency and bond energy, of each bond are calculated using chemical bond theory. The parameters of subformula are calculated by Eqs. (11)–(16) and are listed in Table 3, where the bond lengths used in the calculations are from the experiment data [39]. The calculated covalency (f_c^{μ}) of Al–O bonds (from 0.3819 to 0.5494) is distinctly larger than that of Y–O bonds (from 0.1126 to 0.2871), which is consistent with the Mulliken analysis on the bonds. In addition, the bond energies of Al–O bonds (from 2229 to 2427 kJ·mol^{-1}) are significantly larger than that of Y–O bonds (from 789 to 1162 kJ·mol^{-1}), showing stronger bonding nature of Al–O bonds than that of the Y–O bonds. Among the Y–O bonds, Y(2)–O bonds (bond energies from 1029 to 1132 kJ·mol^{-1}) are stronger than Y(1)–O, Y(3)–O, and Y(4) bonds (bond energies from 789 to 958 kJ·mol^{-1}), because Y(2) is

coordinated by six O atoms, while Y(1), Y(3), and Y(4) atoms are coordinated with seven O atoms. These structural features play an essential role in the elastic and thermal properties of this material, which will be discussed in the following sections.

Table 3 Chemical parameters of subformulas for $Y_4Al_2O_9$ by chemical bond theory

Bond	l^{μ} (Å)	C^{μ} (eV)	E_h^{μ} (eV)	f_i^{μ}	f_c^{μ}	U^{μ} (kJ·mol^{-1})
Y(1)–O(8)	2.2449	14.4162	5.3125	0.8804	0.1196	945.5495
Y(1)–O(7)	2.2854	13.8450	5.0821	0.8813	0.1170	932.3935
Y(1)–O(6)	2.3184	9.3158	4.9051	0.7830	0.2170	927.0889
Y(1)–O(3)	2.3742	12.8372	4.6232	0.8852	0.1148	832.2761
Y(1)–O(1)	2.4195	12.1537	4.4119	0.8836	0.1164	891.2371
Y(1)–O(2)	2.5172	11.0888	3.9994	0.8849	0.1151	863.3986
Y(1)–O(5)	2.6861	9.5186	3.4044	0.8866	0.1134	819.0706
Y(3)–O(2)	2.2563	14.2523	5.2462	0.8807	0.117	941.8106
Y(3)–O(8)	2.2711	14.0432	5.1618	0.88305	0.1193	936.9985
Y(3)–O(8)	2.3429	13.0842	4.7783	0.8823	0.1177	914.3071
Y(3)–O(9)	2.3790	12.6344	4.6005	0.8829	0.1171	903.2929
Y(3)–O(6)	2.5281	10.9777	3.9567	0.8850	0.1150	860.3971
Y(3)–O(5)	2.6436	9.8849	3.5418	0.8862	0.1138	829.8001
Y(3)–O(4)	2.6965	9.4316	3.3719	0.8867	0.1133	816.4864
Y(4)–O(4)	2.2056	15.0006	5.5504	0.8796	0.1204	958.6589
Y(4)–O(9)	2.2883	13.8052	5.0661	0.8813	0.1187	931.4649
Y(4)–O(8)	2.2956	13.7058	5.0263	0.8814	0.1186	929.1352
Y(4)–O(6)	2.3091	13.5245	4.9537	0.8817	0.1183	924.8562
Y(4)–O(9)	2.3826	12.5907	4.5833	0.8830	0.1170	902.2086
Y(4)–O(1)	2.4898	11.3747	4.1094	0.8845	0.1155	871.0341
Y(4)–O(7)	2.8102	8.5450	3.0437	0.8874	0.1126	789.2452
Y(2)–O(1)	2.2426	12.0332	5.3260	0.8362	0.1638	1162.287
Y(2)–O(9)	2.3165	7.7442	4.9145	0.7129	0.2871	1032.688
Y(2)–O(2)	2.3365	10.9495	4.8109	0.8382	0.1618	1125.605
Y(2)–O(3)	2.3395	11.2846	4.7956	0.8470	0.1530	1029.205
Y(2)–O(4)	2.3636	10.6607	4.6752	0.8387	0.1613	1115.430
Y(2)–O(7)	2.3984	10.3013	4.5074	0.8393	0.1607	1102.511
Al(1)–O(3)	1.6562	10.2292	11.2945	0.4506	0.5494	2229.199
Al(1)–O(2)	1.6875	13.3639	10.7821	0.6057	0.3943	2412.366
Al(1)–O(4)	1.7334	12.5967	10.0878	0.6093	0.3907	2368.099
Al(1)–O(5)	1.7788	11.8944	9.4613	0.6125	0.3875	2325.751
Al(2)–O(6)	1.6719	13.6387	11.0333	0.6044	0.3956	2427.754
Al(2)–O(5)	1.7132	12.9269	10.3854	0.6077	0.3923	2387.397
Al(2)–O(7)	1.8083	11.4657	9.0831	0.6144	0.3856	2298.97
Al(2)–O(1)	1.8693	10.6419	8.3657	0.6181	0.3819	2245.354

3. 2 Elastic properties

To disclose the mechanical properties of $Y_4Al_2O_9$, the full sets of independent second-order elastic constants are calculated first. The calculated elastic constants are listed in Table 4. Among all constants, c_{11}, c_{22}, and c_{33} represent the stiffness against principal strains while c_{44}, c_{55}, and c_{66} correspond to resistance to shear deformations. An obvious feature for the elastic constants of $Y_4Al_2O_9$ is that c_{11}, c_{22}, and c_{33} are much higher than c_{44}, c_{55}, and c_{66}, indicating less resistance of $Y_4Al_2O_9$ to the shear deformations.

The calculated elastic constants are used to estimate the mechanical properties, i.e., bulk and shear moduli, Poisson's ratio, and Young's modulus, according to Voigt–Reuss–Hill approximation [20–22]. The calculated mechanical properties are also tabulated in Table 4. To verify the first-principles calculation, the bulk modulus of $Y_4Al_2O_9$ was also estimated using chemical bond theory. The calculated results are listed in Table 5. It is obvious that the bulk moduli for Al–O bonds (from 1145 to 1730 GPa) are enormously larger than those of Y–O bonds (from 118 to 303 GPa), showing less compressibility of Al–O bonds. The bulk modulus for polycrystalline $Y_4Al_2O_9$ is estimated to be 118 GPa, which is lower than the value (132 GPa) calculated by first-principles. The main reason for the low bulk modulus estimated from the chemical bond theory is that large experimental lattice constants from high temperature neutron diffraction [39] were used. If small lattice constants were used, the estimated bulk modulus should be close to the first-principles calculated value.

Shear modulus G describes the resistance of a material against a shape change. As shown in Table 4, the shear modulus of $Y_4Al_2O_9$ is much smaller than bulk modulus. The G/B ratio (namely Pugh's ratio) is 0.576 for $Y_4Al_2O_9$. It is widely accepted that the ductility of a material can be reflected by Pugh's ratio. Ductile materials tend to have a lower value of $G/B <$ 0.571. The Pugh's ratio of SiC, a brittle ceramic, is 0.85 [40], while for the well-known damage tolerant layered ternary carbide and nitride, e.g., Ti_3SiC_2 and Hf_3AlN, they are 0.65 and 0.67, respectively [41]. The Pugh's ratio of $Y_4Al_2O_9$ is lower than those of Ti_3SiC_2 and Hf_3AlN as well as recent recognized damage

Table 4 Second-order elastic constants c_{ij}, anisotropic Young's modulus E_i, and bulk modulus B_H, shear modulus G_H, Young's modulus E, Poisson's ratio ν, Pugh's ratio G/B, and microhardness of $Y_4Al_2O_9$

Second-order elastic constant (GPa)												
c_{11}	c_{22}	c_{33}	c_{44}	c_{55}	c_{66}	c_{12}	c_{13}	c_{15}	c_{23}	c_{25}	c_{35}	c_{46}
251	225	222	74	71	89	79	82	11	88	10	4	–0.5

Anisotropic Young's modulus (GPa)			Elastic moduli (GPa)				G/B and H_V	
E_x	E_y	E_z	B_H	G_H	E	ν	G/B	H_V (GPa)
208	179	176	132	76	191	0.26	0.576	10.21

Table 5 Estimation of bond volume ν^{μ}, lattice energy density μ, bulk modulus *B*, and linear thermal expansion coefficient α of $Y_4Al_2O_9$ using chemical bond theory

Bond	ν^{μ} (Å^3)	μ (GPa)	B^{μ}	α^{μ}	B (GPa)	α (10^{-6}K^{-1})
Y(1)–O(8)	5.64	278	151	8.27	118.08	7.51
Y(1)–O(7)	5.95	260	141	8.42		
Y(1)–O(6)	6.21	248	134	8.76		
Y(1)–O(3)	6.67	207	129	8.77		
Y(1)–O(1)	7.06	209	114	8.96		
Y(1)–O(2)	7.95	180	98	9.35		
Y(1)–O(5)	9.66	141	77	10.02		
Y(3)–O(2)	5.72	273	148	8.31		
Y(3)–O(8)	5.84	266	144	8.37		
Y(3)–O(8)	6.41	237	128	8.65		
Y(3)–O(9)	6.71	223	121	8.79		
Y(3)–O(6)	8.06	177	96	9.39		
Y(3)–O(5)	9.21	150	81	9.85		
Y(3)–O(4)	9.77	139	76	10.06		
Y(4)–O(4)	5.35	297	161	8.11		
Y(4)–O(9)	5.97	259	140	8.44		
Y(4)–O(8)	6.03	256	138	8.47		
Y(4)–O(6)	6.14	250	136	8.52		
Y(4)–O(9)	6.74	222	120	8.81		
Y(4)–O(1)	7.69	188	102	9.24		
Y(4)–O(7)	11.07	118	65	10.72		
Y(2)–O(1)	5.62	343	153	6.70		
Y(2)–O(9)	6.20	303	136	7.18		
Y(2)–O(2)	6.36	294	131	7.02		
Y(2)–O(3)	6.38	268	128	7.02		
Y(2)–O(4)	6.58	281	126	7.11		
Y(2)–O(7)	6.88	266	119	7.23		
Al(1)–O(3)	2.26	1634	436	3.98		
Al(1)–O(2)	2.39	1671	442	3.87		
Al(1)–O(4)	2.60	1514	400	4.00		
Al(1)–O(5)	2.81	1376	364	4.14		
Al(2)–O(6)	2.33	1730	457	3.83		
Al(2)–O(5)	2.51	1581	418	3.95		
Al(2)–O(7)	2.95	1294	342	4.22		
Al(2)–O(1)	3.26	1145	303	4.40		

tolerant oxide ceramics such as ZrP_2O_7 [25], MPO_4 [26], β-$Yb_2Si_2O_7$ [27], and $Yb_3Al_5O_{12}$ [28], revealing low shear deformation resistance and intrinsic damage tolerance of $Y_4Al_2O_9$.

The intrinsic hardness of a material is a highly complex property, which is difficult to describe with a formal theoretical definition. Chen *et al.* [42] proposed an empirical model, which is not only correlated with shear modulus *G*, but also with bulk modulus *B*. In their model, the Vickers hardness is estimated by the following formula:

$$H_{\mathrm{V}} = 2(k^2G)^{0.585} - 3 \tag{24}$$

where *k* is the Pugh's modulus ratio, i.e., *G*/*B*. The Vickers hardness of $Y_4Al_2O_9$ is estimated to be 10.2 GPa, which is close to the experimental measured value of 11.02 GPa [43]. Relatively high hardness indicates that $Y_4Al_2O_9$ is not readily machinable by conventional cutting tools.

The Young's modulus of polycrystalline $Y_4Al_2O_9$ is 191 GPa according to Eq. (1). The anisotropic Young's moduli along three principle directions are $E_x = 208$ GPa, $E_y = 179$ GPa, and $E_z = 176$ GPa, respectively, showing anisotropic elastic behavior of $Y_4Al_2O_9$. The anisotropic Young's moduli are reflections of chemical bonding within the crystal structure of $Y_4Al_2O_9$. To visually demonstrate the anisotropic crystal structure of $Y_4Al_2O_9$, the projection of atoms on (010) and (100) planes are shown in Fig. 1(b) and Fig. 1(c), respectively. From Fig. 1(b), one can see that corner-shared AlO_4 tetrahedra align almost parallel to *x* direction. Since the bonding in AlO_4 tetrahedron is much stronger than the Y–O polyhedra (Table 2, Table 3, and Table 5), the Young's modulus in *x* direction is much higher than those in *y* and *z* directions. To obtain a clear and complete representation of the elastic anisotropy of $Y_4Al_2O_9$, the variation of Young's modulus as a function of crystal orientation is necessary. The direction dependence of Young's modulus, *E*, for $Y_4Al_2O_9$ is given by the following equation [44]:

$$\begin{aligned}\frac{1}{E} = {} & l_1^4 s_{11} + 2l_1^2 l_2^2 s_{12} + 2l_1^2 l_3^2 s_{13} + 2l_1^3 l_3 s_{15} + l_2^4 s_{22} \\ & + 2l_2^2 l_3^2 s_{23} + 2l_1 l_2^2 l_3 s_{25} + l_3^4 s_{33} + 2l_1 l_3^3 s_{35} + l_2^2 l_3^2 s_{44} \\ & + 2l_1 l_2^2 l_3 s_{46} + l_1^2 l_3^2 s_{55} + l_1^2 l_2^2 s_{66}\end{aligned} \tag{25}$$

where s_{ij} is the elastic compliance; l_1, l_2, and l_3 are the directional cosines of angles with the three principle directions, respectively.

The surface contour of the Young's modulus of $Y_4Al_2O_9$ is shown in Fig. 2(a), and the planar projection of Young's modulus for (100), (010), and (001) crystallographic planes are shown in Fig. 2(b). For different crystallographic planes, A, B, and C directions represent different crystallographic directions: for (001) plane, A direction represents [100] and B represents [010]; for (010) plane, B represents [001] and C represents [100]; for (100) plane, A represents [010] and B represents [001]. The elastic anisotropy of $Y_4Al_2O_9$ is clearly illustrated. The anisotropy of Young's modulus on (010) plane is much stronger than that on the (100) and (001) planes. The maximum Young's modulus is 210 GPa, which is parallel to the direction of corner-shared AlO_4 tetrahedra; while the minimum Young's modulus is 170 GPa, parallel to $[0\bar{1}1]$ direction. The high- and low-directions correspond to the high- and

low-fracture-energy directions. Figure 2 shows the anisotropy of the elastic properties of $Y_4Al_2O_9$ and it is also an indication of the expected low- and high-fracture-energy directions in the crystal. With this information, the most important directions for mechanical property measurements and applications can be evaluated.

3. 3 Thermal properties

Thermal expansion coefficient (TEC), resulted from the anharmonic vibration of the lattice at a finite temperature, is a fundamental parameter characterizing a material. Theoretical evaluation on TEC is quite a challenge for material scientists. Several approaches including quasi-harmonic approximation (QHA) [45], molecular dynamics (MD) [46], and chemical bond theory [37] have been proposed to estimate TEC theoretically. The chemical bond theory proposed by Zhang *et al.* [37] is a simple empirical method to predict the average linear expansion coefficients of complex crystals based only on the crystal structure data. However, their calculated results show excellent agreement with the experimental values. Therefore, the linear expansion coefficient of $Y_4Al_2O_9$ was evaluated by chemical bond theory in this work. The calculated results are listed in Table 5. Considering that the bond strength of Al–O bonds is substantially stronger than that of Y–O bonds, it is not surprising that the contribution from Al–O bonds is quite smaller than that from Y–O bonds. The expansion coefficient of $Y_4Al_2O_9$ is 7.51×10^{-6} K^{-1}, theoretically. Experimentally, the TEC of $Y_4Al_2O_9$ is 7.37×10^{-6} K^{-1} [43], which is quite close to the theoretical one, demonstrating the reliability of the theoretical result.

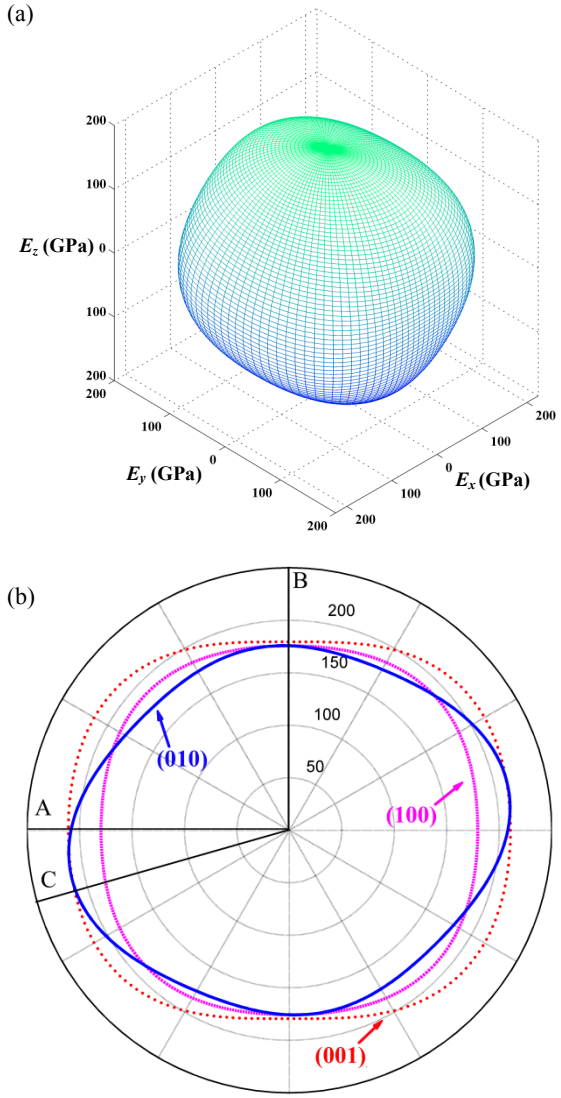

Fig. 2 (a) Surface contour of direction dependent Young's modulus of $Y_4Al_2O_9$; (b) planar projections on (001), (100), and (010) crystallographic plane.

The behavior of thermal transportation at different temperature ranges is an important factor that needs to be considered when selecting an applicable TBC. As shown in Eqs. (3) and (5), estimation of the intrinsic thermal conductivity of $Y_4Al_2O_9$ relies on the knowledge of sound velocities (υ_l, υ_s, υ_m), Debye temperature (Θ_D), and Grüneisen parameter (γ). The sound velocities and Debye temperature are derived from DFT calculated elastic moduli and density of equilibrium structure by Eqs. (6)–(8). The calculated parameters for $Y_4Al_2O_9$ are listed in Table 6.

At relatively high temperatures, the dominant mechanism of phonon scattering, which determines the intrinsic lattice thermal conductivity of a material, is the Umklapp processes, in which the acoustic phonon branches interact with each other to transport heat. Slack's model (i.e., Eq. (3)) [8] is a suitable approach to describe the temperature dependence of thermal conductivity when the Umklapp scattering is dominant. The temperature dependence of thermal conductivity of $Y_4Al_2O_9$ estimated from Slack's model is shown in Fig. 3. The thermal conductivity of $Y_4Al_2O_9$ decreases with temperature. With the further increase in temperature, the thermal conductivity would approach

Table 6 Sound velocities υ_l, υ_s, and υ_m, Debye temperature Θ_D, Grüneisen parameter γ, and minimum thermal conductivity of $Y_4Al_2O_9$

υ_l (km·s^{-1})	υ_s (km·s^{-1})	υ_m (km·s^{-1})	Θ_D (K)	γ	κ_{min} (W·m^{-1}·K^{-1})
7.02	4.00	4.45	564	1.55	1.12

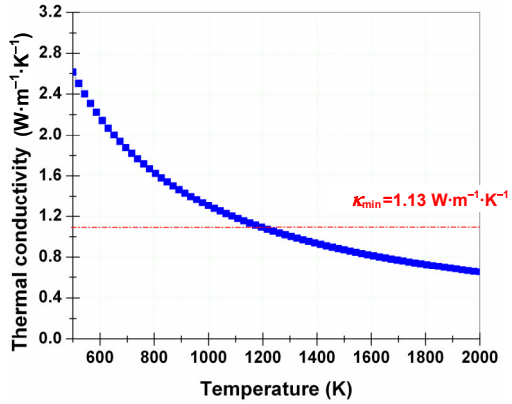

Fig. 3 Temperature dependence of thermal conductivity of $Y_4Al_2O_9$. Theoretical minimum thermal conductivity (red dash line) is also shown.

a minimum when the phonon mean-free path decreased to the average atomic distance [13]. The minimum thermal conductivity κ_{min} can be evaluated by modified Clarke's model, as illustrated by Eqs. (5) and (6). The minimum thermal conductivity of $Y_4Al_2O_9$ was predicted to be 1.13 $W \cdot m^{-1} \cdot K^{-1}$. Combining these two models, the behavior of thermal transportation of $Y_4Al_2O_9$ can be described as follows. With the increasing of temperature, the thermal conductivity of $Y_4Al_2O_9$ declines as $\kappa = 1305.6 / T$, and it reaches a minimum value at around 1150 K and keeps almost unchanged with further temperature increase.

Low minimum thermal conductivity (1.13 $W \cdot m^{-1} \cdot K^{-1}$ for $Y_4Al_2O_9$) has been predicted and proved in many oxide ceramics like ZrP_2O_7 (1.15 $W \cdot m^{-1} \cdot K^{-1}$) [25], α-$AlPO_4$ (1.02 $W \cdot m^{-1} \cdot K^{-1}$) [26], β-$Yb_2Si_2O_7$ (1.12 $W \cdot m^{-1} \cdot K^{-1}$) [27], $Yb_3Al_5O_{12}$ (1.22 $W \cdot m^{-1} \cdot K^{-1}$) [28], and Yb_2SiO_5 (0.74 $W \cdot m^{-1} \cdot K^{-1}$) [29]. The low thermal conductivity of these oxides can be traced back to their structural characteristics. The origin of such low thermal conductivity is mainly attributed from the heterogeneous bond strength. Rigid units like SiO_4, PO_4, and AlO_4 are efficient in phonon transport, while weakly bonded unit like YbO_6 intensifies the scattering of phonon. In $Y_4Al_2O_9$, the softer Y–O polyhedra are equivalent to the thermal rattle structures, and provide "weak zones" that scatter phonons and reduce phonon mean-free path. In addition, as suggested by Clarke [11], the strongest influence on the minimum thermal conductivity is the ratio of the atomic weight to the number of atoms per molecule, i.e., mean atomic weight M/n in Eq. (5). The relatively high mean atomic weight of $Y_4Al_2O_9$ is 39.93 amu/atom, which results in the low thermal conductivity of $Y_4Al_2O_9$.

4 Conclusions

In this work, the chemical bonding characteristics, elastic stiffness, thermal expansion coefficient, and thermal conductivity of $Y_4Al_2O_9$ were investigated by first-principles calculations and chemical bond theory. The theoretical results reveal the heterogeneous bonding nature of $Y_4Al_2O_9$, i.e., Al–O bonds are stronger than Y–O bonds. The second-order elastic constants and mechanical properties of $Y_4Al_2O_9$ were calculated. The low G/B ratio suggests that the shear deformation resistance of $Y_4Al_2O_9$ is relatively low and damage tolerance is expected in this ceramic. The hardness is estimated to be 10.2 GPa from the DFT calculated elastic moduli. $Y_4Al_2O_9$ shows anisotropy in elastic behavior based on the discussion of direction dependence of Young's modulus. Using chemical bond theory, the TEC of $Y_4Al_2O_9$ is estimated to be 7.51×10^{-6} K^{-1}. The temperature dependence of thermal conductivity of $Y_4Al_2O_9$ is predicted based on the obtained elastic moduli, sound velocities, and Debye temperature. The intrinsic thermal conductivity of $Y_4Al_2O_9$ decreases as $1305.6/T$ and approaches a minimum thermal conductivity (1.13 $W \cdot m^{-1} \cdot K^{-1}$) at high temperatures. Weak Y–O bonds and large mean atomic weight contribute to the low thermal conductivity of $Y_4Al_2O_9$. The unique combination of low thermal conductivity, moderate thermal expansion coefficient, and damage tolerance highlights the potential of $Y_4Al_2O_9$ as a promising candidate material for thermal barrier coating applications.

Acknowledgements

This work was supported by the National Outstanding Young Scientist Foundation for Y. C. Zhou under Grant No. 59925208, and the National Natural Science Foundation of China under Grant Nos. 50832008 and U1435206.

References

[1] Slifka AJ, Filla BJ, Phelps JM, *et al*. Thermal conductivity

of a zirconia thermal barrier coating. *J Therm Spray Techn* 1998, **7**: 43–46.
[2] Miller RA, Smialek JL, Garlick RG. Phase stability in plasma sprayed partially stabilized zirconia–yttria. In *Advances in Ceramics*, *Vol. 3*, *Science and Technology of Zirconia*. Heuer AH, Hobbs LW, Eds. Columbus, OH: American Ceramic Society, 1981: 241–251.
[3] Clarke DR, Levi CG. Materials design for the next generation thermal barrier coatings. *Annu Rev Mater Res* 2003, **33**: 383–417.
[4] Clarke DR, Phillpot SR. Thermal barrier coating materials. *Mater Today* 2005, **8**: 22–29.
[5] Harada Y, Suzuki T, Hirano K, *et al*. Environmental effects on ultra-high temperature creep behavior of directionally solidified oxide eutectic ceramics. *J Eur Ceram Soc* 2005, **25**: 1275–1283.
[6] Djemia P, Tétard F, Bouamama K, *et al*. Elasticity and lattice vibrational properties of transparent polycrystalline yttrium–aluminium garnet: Experiments and pair potential calculations. *J Eur Ceram Soc* 2007, **27**: 4719–4725.
[7] Zhan X, Li Z, Liu B, *et al*. Theoretical prediction of elastic stiffness and minimum lattice thermal conductivity of $Y_3Al_5O_{12}$, $YAlO_3$ and $Y_4Al_2O_9$. *J Am Ceram Soc* 2012, **95**: 1429–1434.
[8] Mah T-I, Petry MD. Eutectic composition in the pseudobinary of $Y_4Al_2O_9$ and Y_2O_3. *J Am Ceram Soc* 1992, **75**: 2006–2009.
[9] Zhou X, Xu Z, Fan X, *et al*. $Y_4Al_2O_9$ ceramics as a novel thermal barrier coating material for high temperature applications. *Mater Lett* 2014, **134**: 146–148.
[10] Li Z, Liu B, Wang JM, *et al*. First-principles study of point defects in stoichiometric and nonstoichiometric $Y_4Al_2O_9$. *J Mater Sci Technol* 2013, **29**: 1161–1165.
[11] Clarke DR. Materials selection guidelines for low thermal conductivity thermal barrier coatings. *Surf Coat Technol* 2003, **163–164**: 67–74.
[12] Liu B, Wang JY, Li FZ, *et al*. Theoretical elastic stiffness, structural stability and thermal conductivity of $La_2T_2O_7$ (T = Ge, Ti, Sn, Zr, Hf) pyrochlore. *Acta Mater* 2010, **58**: 4369–4377.
[13] Slack GA. Nonmetallic crystals with high thermal conductivity. *J Phys Chem Solids* 1973, **34**: 321–335.
[14] Segall MD, Lindan PJD, Probert MJ, *et al*. First-principles simulation: Ideas, illustrations and the CASTEP code. *J Phys*: *Condens Matter* 2002, **14**: 2717–2743.
[15] Vanderbilt D. Soft self-consistent pseudopotential in a generalized eignevalue formalism. *Phys Rev B* 1990, **41**: 7892–7895.
[16] Ceperley DM, Alder BJ. Ground state of the electron gas by a stochastic method. *Phys Rev Lett* 1980, **45**: 566–569.
[17] Monkhorst HJ, Pack JD. Special points for Brillouin-zone integrations. *Phys Rev B* 1976, **13**: 5188–5192.
[18] Pfrommer BG, Côté M, Louie SG, *et al*. Relaxation of crystals with the quasi-Newton method. *J Comput Phys* 1997, **131**: 233–240.
[19] Milman V, Warren MC. Elasticity of hexagonal BeO. *J Phys*: *Condens Matter* 2001, **13**: 241–245.
[20] Voigt W. *Lehrbuch der Kristallphysik*. Taubner, Leipzig: Johnson Reprint Corp, 1928.
[21] Reuss A. Berechnung der Fließgrenze von Mischkristallen auf Grund der Plastizittsbedingung für Einkristalle. *Z Angew Math Mech* 1929, **9**: 49–58.
[22] Hill R. The elastic behaviour of a crystalline aggregate. *Proc Phys Soc A* 1952, **65**: 349–354.
[23] Green DJ. *An Introduction to the Mechanical Properties of Ceramics*. Cambridge: Cambridge University Press, 1993.
[24] Sanditov BD, Tsydypov SB, Sanditov DS. Relation between the Grüneisen constant and Poisson's ratio of vitreous system. *Acoust Phys*+ 2007, **53**: 594–597.
[25] Xiang H, Feng Z, Zhou Y. *Ab initio* computations of electronic, mechanical, lattice dynamical and thermal properties of ZrP_2O_7. *J Eur Ceram Soc* 2014, **34**: 1809–1818.
[26] Zhou Y, Liu B. Theoretical investigation of mechanical and thermal properties of MPO_4 (M = Al, Ga). *J Eur Ceram Soc* 2013, **33**: 2817–2821.
[27] Zhou Y-C, Zhao C, Wang F, *et al*. Theoretical prediction and experimental investigation on the thermal and mechanical properties of bulk β-$Yb_2Si_2O_7$. *J Am Ceam Soc* 2013, **96**: 3891–3900.
[28] Zhou Y, Xiang H, Feng Z. Theoretical investigation on mechanical and thermal properties of a promising thermal barrier material: $Yb_3Al_5O_{12}$. *J Mater Sci Technol* 2014, **30**: 631–638.
[29] Xiang H, Feng Z, Zhou Y. Mechanical and thermal properties of Yb_2SiO_5: First-principles calculations and chemical bond theory investigations. *J Mater Res* 2014, **29**: 1609–1619
[30] Anderson OL. A simplified method for calculating the Debye temperature from elastic constants. *J Phys Chem Solids* 1963, **24**: 909–917.
[31] Phillips JC, Van Vechten JA. Dielectric classification of crystal structures, ionization potentials, and band Structures. *Phys Rev Lett* 1969, **22**: 705.
[32] Van Vechten JA. Quantum dielectric theory of electronegativity in covalent systems. I. Electronic dielectric constant. *Phys Rev* 1969, **182**: 891.
[33] Levine BF. Bond susceptibilities and ionicities in complex crystal structures. *J Chem Phys* 1973, **59**: 1463.
[34] Xue D, Zhang S. Calculation of the nonlinear optical coefficient of the $NdAl_3(BO_3)_4$ crystal. *J Phys*: *Condens Matter* 1996, **8**: 1949–1956.
[35] Liu D, Zhang S, Wu Z. Lattice energy estimation for inorganic ionic crystals. *Inorg Chem* 2003, **42**: 2465–2469.
[36] Zhang S, Li H, Li H, *et al*. Calculation of the bulk modulus of simple and complex crystals with the chemical bond method. *J Phys Chem B* 2007, **111**: 1304–1309.
[37] Zhang S, Li H, Li L, *et al*. Calculation of bulk modulus on carbon nitrides with chemical bond method. *Appl Phys Lett* 2007, **91**: 251905.
[38] Zhang S, Li H, Zhou S, *et al*. Estimation thermal expansion coefficient from lattice energy for inorganic crystals. *Jpn J Appl Phys* 2006, **45**: 8801–8804.
[39] Yamane H, Shimada M, Hunter BA. High temperature neutron diffraction study of $Y_4Al_2O_9$. *J Solid State Chem* 1998, **141**: 466–474.

[40] Lambrecht WRL, Segall B, Methfessel M, *et al*. Calculated elastic constants and deformation potentials of cubic SiC. *Phys Rev B* 1991, **44**: 3685–3694.

[41] Li F, Liu B, Wang J, *et al*. Hf_3AlN: A novel layered ternary ceramic with excellent damage tolerance. *J Am Ceram Soc* 2010, **93**: 228–234.

[42] Chen X-Q, Niu HY, Li DZ, *et al*. Modeling hardness of polycrystalline materials and bulk metallic glasses. *Intermetallics* 2011, **19**: 1275–1281.

[43] Zhou Y, Lu X, Xiang H, *et al*. Preparation, mechanical, and thermal properties of a promising thermal barrier material: $Y_4Al_2O_9$. *J Adv Ceram* 2015, DOI: 10.1007/s40145-015-0141-5.

[44] Nye JF. *Physical Properties of Crystals*: *Their Representation by Tensors and Matrices*. Oxford: Oxford Science Publications, 1985.

[45] Blanco MA, Francisco E, Luaña V. GIBBS: Isothermal–isobaric thermodynamics of solids from energy curves using a quasi-harmonic Debye model. *Comput Phys Commun* 2004, **158**: 57–72.

[46] Car R, Parrinello M. Unified approach for molecular dynamics and density-functional theory. *Phys Rev Lett* 1985, **55**: 2471–2474.